Materials Science

http://www.aimspress.com/journal/Materials/

AIMS Materials Science, 4(2): 340-362.
DOI: 10.3934/matersci.2017.2.340
Received: 05 October 2016
Accepted: 27 December 2016
Published: 20 February 2017

Research article

Electrical properties of covalently functionalized graphene

Paul Plachinda*, **David Evans, and Raj Solanki**

Department of Physics, Portland State University, 1719 SW 10th Ave., Portland, OR 97201, USA

* **Correspondence:** Email: solanki@pdx.edu; Tel: +1-503-725-3231; Fax: +1-503-725-2815.

Abstract: We have employed first-principle calculations to study transformation of graphene's electronic structure under functionalization by covalent bonds with different atomic and molecular groups - epoxies, amines, PFPA. It is shown that this functionalization leads to an opening in the graphene's band gap on order of tens meV, but also leads to reduction of electrical conductivity. We also discuss the influence of charge exchange between the functionalizing molecule and graphene's conjugated electrons on electron transport properties.

Keywords: graphene; functionalization; DFT; PFPA; amines; epoxy

1. Introduction

Currently, the digital logic devices are composed almost entirely of the silicon field-effect transistors because silicon has a band gap that allows the devices to be turned on and off to produce the digital signals. As the scaling of these devices is approaching its limits, the industry is adopting more complex structures such as the multi-gated FinFETs to extend the life of the silicon transistor technology by a few more generations. Beyond that, an alternative to silicon will be required and among the candidates considered to replace silicon is graphene. As with most semiconductors, the band structure and hence the electronic properties of a material depend on the arrangement of its atoms. However, unlike most semiconductors, the monolayered C atoms of graphene are arranged in 2-dimensional, honeycomb lattice structure. As a result, this material has unique mechanical and electrical properties, including high carrier mobility. However, graphene does not possess a bandgap, i.e., it is a semi-metal so it cannot readily be used to fabricate field-effect transistors. Therefore there is an active effort to determine a way to induce a bandgap in graphene, while conserving its desirable properties, especially the high carrier mobility. One of the ways to produce aband gap and maintain high mobility in graphene is by functionalization, namely bonding covalent (or e.g. haptic) molecules to its surface.

Chemical modification of graphene by covalent functionalization of its surface potentially allows

a wider flexibility in engineering of the electronic structure, in particular, the local density of states of the carbon atoms bound to the modifier, that can result in opening of a band gap. Such binding can involve covalent hydrogenation of graphene to modify hybridization of carbon atoms from sp^2 to sp^3 geometry [1, 2, 3]. Methods have also been developed to functionalize graphene covalently with molecular species [4, 5, 6, 7, 8]. Among these, perfluorophenylazide (PFPA) functionalization of graphene is well-developed using a nitrene intermediate. Films of this molecule act as adhesion layers to produce long ribbons of exfoliated graphene [7, 8, 9].

2. Covalent Bonding to Graphene

A great deal of interest in covalent functionalization of graphene (CFGR) was generated when it was shown that functionalized graphene can act as a sensor by changing its electronic properties (conductivity at first), depending on the number and the type of adsorbed molecules. Some initial attempts have already been made to induce charge carriers into graphene by means of the adsorption of various gas molecules including NH_3, H_2O, and NO_2 and to study how it affects the density of states (DoS) [10, 11, 3], which is related to conductivity, electron energy loss, and X-ray photoelectron spectra. Primary interest in any functionalization depends on whether a functionalizing molecule acts like an electron donor, or as an electron acceptor, i.e., if the charge of an atom bound to a graphene sheet is increased or decreased compared to the functionalizing molecule in the free state.

Despite a detailed analysis of the density of states (DoS) and band structure of graphene sheets functionalized with "small molecules" (like NH_3, H_2O, NO_2, NO, CO [10, 11, 12], transition metals [13]), and "large molecules" (like porphyrines and buckyballs [4], azido-trimethyl-silane [5], azomethine [6]), very little theoretical [14, 15, 16] and experimental [17, 18] attempts have been made to study electrical conductance of those structures.

The choice of heteroatoms (labeled as X in tables and formulas) for covalent functionalization of graphene is limited by their electronic structure: hydrogen and halogen atoms have only one vacancy in their electron shell and thus can bind to p_z orbitals, the only binding spot for halogens can be on the edge of a graphene nano ribbon (GNR).

Chalcogens (O, S) have six valence electrons, thus radicals like **R-:Ṡ:**, when bound to graphene tend to reconstruct to **...-C-:S:-C-...** with two saturated lone pairs, which are chemically inert, hence no further functionalization is possible with chalcogens. Therefore epoxygraphene and thioethergraphene are the only possible varieties of graphene functionalized compounds with chalcogen atoms.

Group V elements with five valence electrons can also bind to two graphene carbon atoms. In this case e.g. a nitrene radical **R-N̈:** after binding to graphene reconstructs to **...-C-Ṅ:-C-...**, where unlike chalcogenes, the dangling bond (one unshared electron) is highly reactive and can bind to various other radicals, the simplest of which is a hydrogen atom. This will form an aminographene.

Besides nitrogen in amines other heteroatom subsituents can be used for functionalization. Phosphinidene radical (**R-P̈:**) is a direct analog of nitrene, therefore everything said above about electron configuration and geometry of nitrene can be used to describe phosphinidene, while noticing that the larger size of the P atom can produce more sterical congestions for the molecule. Carbene (**R–C̈–R**) derivatives can bind to graphene in two ways: leaving a single lone pair or saturating it with hydrogen or bigger molecules. In the first case carbene functionalized graphene would be represented as **...C–C̈–C...**, in the second one, however, as **...C–RCR–C...**. The first case is similar to epoxy- and

epthographene and is considered together with them, the second is considered along with other structures with the same moieties. An electron deficient boranylidene (**R-B:**) radical can also bind to a graphene sheet, where we can expect an upright geometry of the substituent due to absence of the lone pairs and weaker electrophilic properties.

Thus, there is an "ep"-group of functioinalizing atoms (O, S, C), that cannot bind to anything else, and the $\dot{B}$, CH_2, $\dot{N}$, $\dot{P}$, etc. - based substituents, that have one unsaturated valence bond and thus can be attached to a hydrogen atom or to further more complex substituents like e.g. PFPA*.

In the next section, band structure and conductivity studies of an ep-functionalized graphene will be considered. The choice of the structure is dictated by its relative simplicity, along with didactic usefulness, and understanding of key concepts of covalent functionalization. The calculations were conducted within the framework of the density function theory (DFT) as implemented in the $DMol^3$ package[19]. The generalized gradient approximation (GGA) in BLYP [20, 21] exchange-correlation parameterization was used for both final geometry optimization and band structure calculation. Initial geometry optimization was performed using the local density approximation (LDA) approximation with the Vosko-Wilk-Nusair (VWN) [22] correlation functional.

A 6x6 graphene supercell with a vacuum space of 11.5Å normal to graphene plane was used. Geometry optimization convergence criterion was satisfied when the total energy change was less than of 3×10^{-5} Ha. Only one k-point (Γ) was used throughout the structural calculations since the distance between neighboring k-points was only 0.077 1/Å due to a large supercell choice. For the band structure computation the k-path selected was Γ-M-K-Γ with 24, 20, and 40 k-points on each segment correspondingly.

3. Ep-Functionalization

In this section we shall discuss the "ep"-functionalized graphene. Under "ep" we will consider all kinds of structures that appear by functionalization of a graphene sheet with chalcogenes and C atoms. Hereinafter they are labeled as (O,S,C,..)-epgraphene.

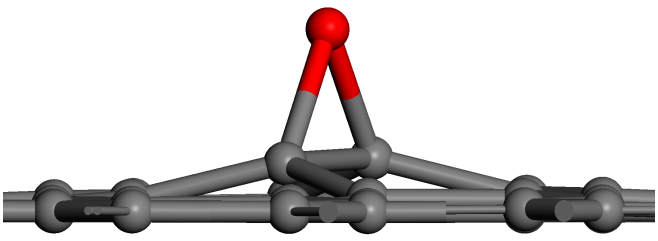

Figure 1. Fragment of the optimized structure of epoxy functionalized graphene (O-epgraphene). Carbon atoms are gray, oxygen -red.

The structure of epoxygraphene was first optimized as described in the section above. As a result of geometrical optimization a deplanarization of two carbon atoms occurred, adjoining the function-

*Its particular applicability will be discussed later

alizing chalcogen atom. This deplanarization is linked to the partial rehybridization of carbon atoms changing their electronic structure from pure sp^2 to $sp^2 + sp^3$. No complete rehybridization occurs for these atoms because the angle of the C–C bond still remains much less than 109°. A general $sp^{2+\eta}$ hybridization is expected to have a higher excitation energy than that of the symmetric sp^2 hybridization discussed before, because of the electron- electron repulsion which occurs in the hybridized orbital [23]. Comparing the bond length in C-,O-, and S-epgraphene, one can see that the shortest C–X distance ($d(C - X)$) is observed when X=O, which is the most electronegative atom in the C, O, S row. Therefore C-O bond is the strongest. However, due to its high electronegativity, donor properties of the oxygen atom are relatively weak compared to sulfur. Therefore the highest charge transfer occurs in S-epgraphene. This enhanced charge transport leads to the the strongest disturbance of the π-conjugated electron system of graphene for the given class of fuctionalizing compounds. Hence, additional electron donation manifests itself in stronger rehybridization and band gap opening in S-epgraphene. However, the degree of rehybridization (η) is fairly low in these structures: the molecular orbitals (MO) and Wannier functions (WF) pictures reveal that the states near the Fermi level are primarily constructed from graphene conjugated π orbitals without significant admixture of the states from the heteroatom. (See Figs.3, 4)

3.1. Band structure of epoxygraphene

For the bandgap calculation we chose the configuration of one functionalizing atom per a 6x6 graphene supercell. Usually higher functionalization degrees lead to stronger discrepancy between the diagonal element of the Hamiltonian matrix.

From the tight binding description of the band structure of graphene [24] if two carbon atoms in the unit cell are not equivalent (as it happens in graphite due to an offset of the next layer), an energy gap of magnitude $E_g \sim |H_{11} - H_{22}|$ occurs between the valence and the conductive bands. (H_{11} and H_{22} are the diagonal elements of the Hamiltonian matrix in the Tight Binding Approximation (TBA)). Therefore, everything that makes the atoms nonequivalent opens a band gap in graphene. Every functionalizing group disturbs in some way the electronic structure of the atom it is bound to, making the diagonal elements of the Hamiltonian matrix nonequivalent. Moreover, the stronger the disturbance of the local electronic structure, the wider is the gap. If the functionalization does not occur to one of the three nearest neighbors, the TBA can be expanded by including more terms in the Hamiltonian matrix in the secular equation. However, as long as at least one H_{jj} coefficient is not equal to all other diagonal elements, a gap will be opened. Thus the value of the band gap will also change not only with the type of functionalizing molecule, but also with the ratio of the functionalized carbon atoms to the untouched ones. This model provides transparent physical background for functionalization of graphene.

As presented below, the band gaps are so narrow, that only a very excessive functionalization can create a band gap which is at least four times the thermal energy at room temperature. However, excessive functionalization with oxygen atoms (each honeycomb in a row functionalized) is known to cause ”unzipping” and cracking of graphene sheets [25].

Numerical values of band gaps are summarized in Table 2 at the end of the paper. Band gaps vary from 39meV for epoxygraphene to 41 meV for epthiographene. Bandgaps increase as the charge transfer of the corresponding atom increases. Atomic Mulliken charges follow the same trend as band gaps do: -0.411e for epoxygraphene, -0.247e for epthiographene, and -0.025e for epcarbographene. The more electrons a heteroatom is able to donate or accept from the π-conjugated system (i.e. the

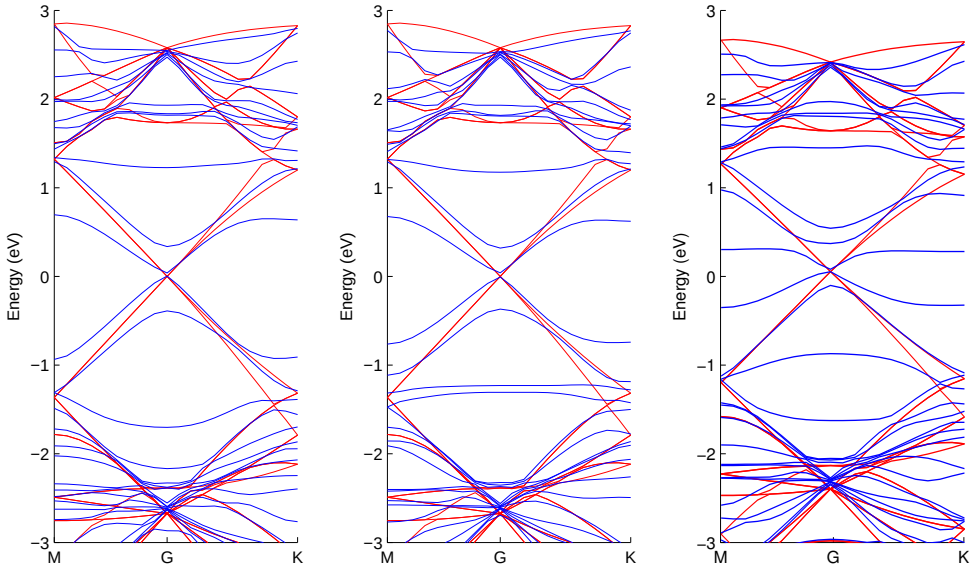

(a) O-epgraphene **(b) S-epgraphene** **(c) C-epgraphene**

Figure 2. Band structures of pristine (red) and ep-functionalized (blue) graphene. Band structures were aligned with respect of the position of the Fermi level.

larger the charge transfer), the more disturbance it causes in the conjugated system, and therefore, the higher is the difference between the diagonal elements of the Hamiltonian matrix. However, these bandgaps are still about the thermal energy at room temperature. Therefore ep- functionalization of graphene is most likely a dead end. But for didactic and benchmarking purposes, transport calculation for epoxygraphene are presented in the section below.

3.2. Wannier functions and transport in epoxygraphene

For the transport computations a fairly large (6x6) supercell is chosen, consisting of 85 atoms per unit cell, where the total number of bands considered in the non self-consistent field (nSCF) calculation was set at 800[†]. SCF computation is conducted on a 3 3 1 MP grid, nSCF - on 9 k-points in the whole BZ. The size of the supercell allowed not to conduct separate computation of the semi-infinite electrodes, but rather to assume that the Wannier functions far away (about 3 honeycombs) from the functionalizing atom are not disturbed by functionalization and thus can be taken as the electrodes' Wannier functions. An advantage of this scheme is that the Fermi levels in the conductor region and the electrodes are matched automatically. Also, since the width of practical graphene nanoribbons are often on the order of 1μm, we may assume bulk conductivity mode for all structures under consideration.

Trial Wannier functions (WF) were initialized as two subsets: graphene subset is initialized as a set of σ-type orbitals located between carbon atoms and dangling p_z orbitals. The subsets of heteroatoms are explicitly defined as their atomic orbital set (1s+3p orbitals). Binding to the graphene sheet is achieved by mixing of p_z orbitals of carbon atoms adjoined to the heteroatom and its s atomic orbitals

[†]This number is obtained from the rule of thumb that for good convergence the number of empty band considered should be three times of the number of the occupied ones

(AO) (Fig. 3). Other AOs of the heteroatom (p_x, p_y, p_z) do not participate in the bonding process: p_x and p_y remain undistorted and only slight interaction is observed with π-system of graphene (Fig. 4(a)), p_z does not participate at the bonding process forming the lone pair (Fig. 4(b)).

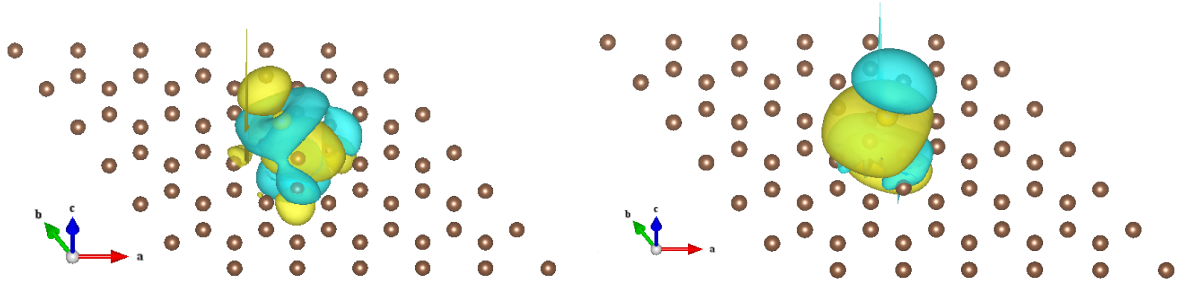

(a) p_z **(b)** s

Figure 3. Wannier functions of S-epgraphene. Binding set.

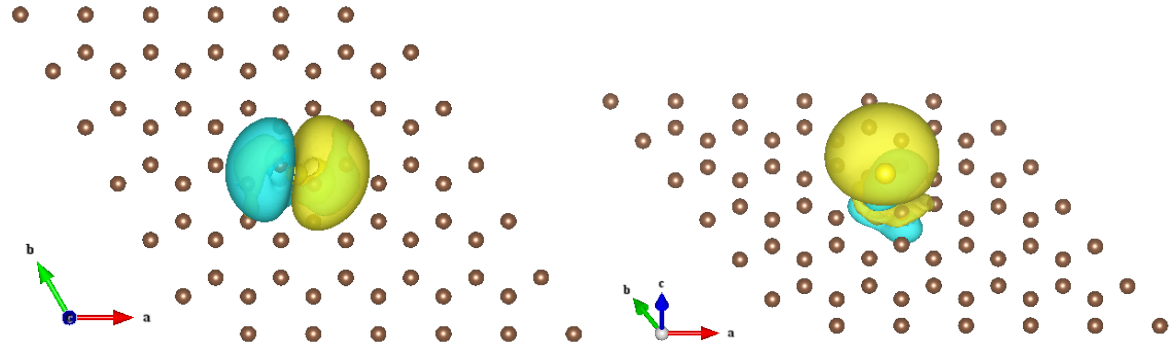

(a) p_x **or** p_y **(b)** p_z

Figure 4. Wannier functions of S-epgraphene. Nonbinding set.

The WF picture confirms very weak interaction between the heteratoms and the electron system of graphene. The HOMO consists entirely of graphene π orbitals, whereas the doubly degenerate LUMO consists of the p_x and p_y orbitals of the heteroatom. Absence of mixing allows to represent the Hamiltonian matrix of the system in the block diagonal form, so that the eigenvector problem almost splits into two independent subsets of secular equations. Therefore, the diagonal elements of the graphene block of the Hamiltonian matrix are almost undisturbed by ep-funtionalization. This fact also manifests itself in the transport properties: conductance of epgraphene (Fig. 5) closely resembles that of pristine graphene, and differ from that only due to presence of additional states imposed by the heteroatom and folding of the BZ.

As it can be seen from Fig. 5, the highest conductivity occurs in S-epgraphene. The trend in conductance (see Fig. 5 and table 2) follows the trend in the band gap. The reason for that is that since epgraphene has very little mixing of AOs, its band structure can be split into ”graphene bands” and ”heteroatom bands”, which would bring the Hamiltonian matrix to the block-diagonal shape. Since the determinant of a block-diagonal matrix is a product of the determinants of the corresponding blocks, conductance calculated from that matrix can be represented as two sums as well. Also because of the very little mixing, the heteroatom energy levels possess very small dispersion, and thus the electrons,

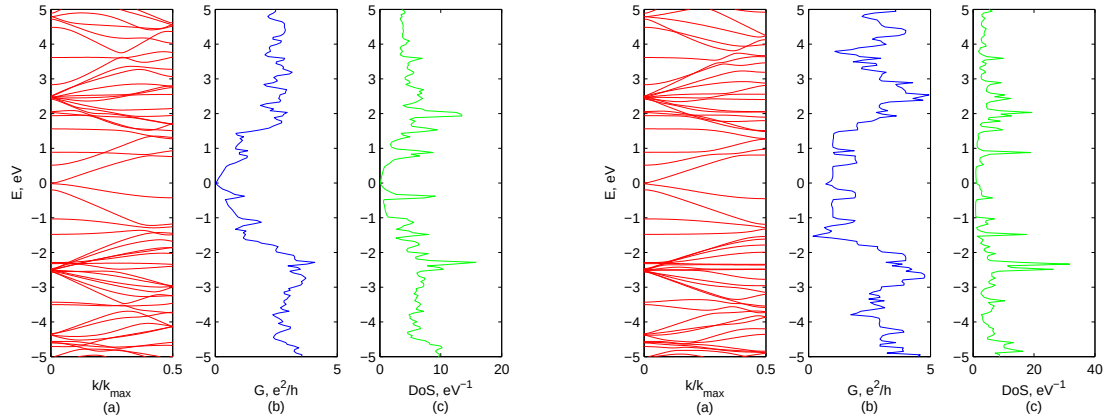

C-ep in Γ-K direction **C-ep in Γ-M direction**

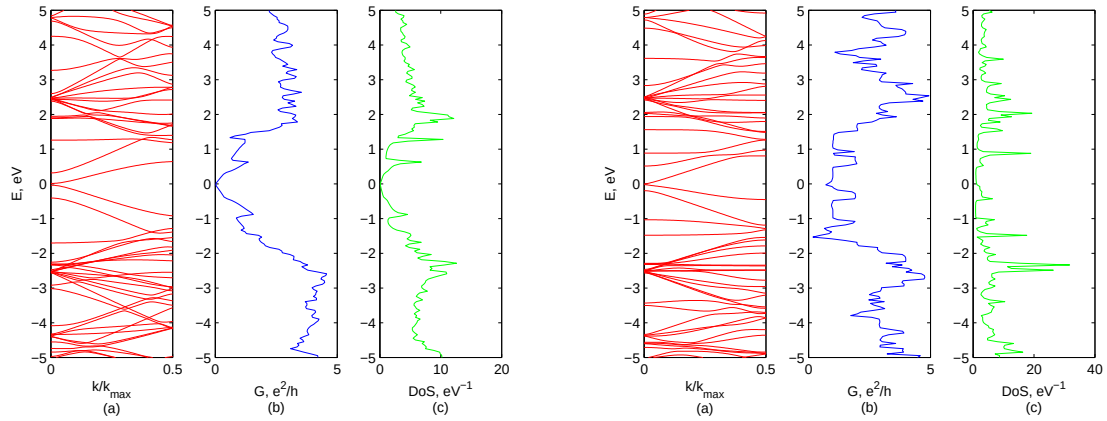

O-ep in Γ-K direction **O-ep in Γ-M direction**

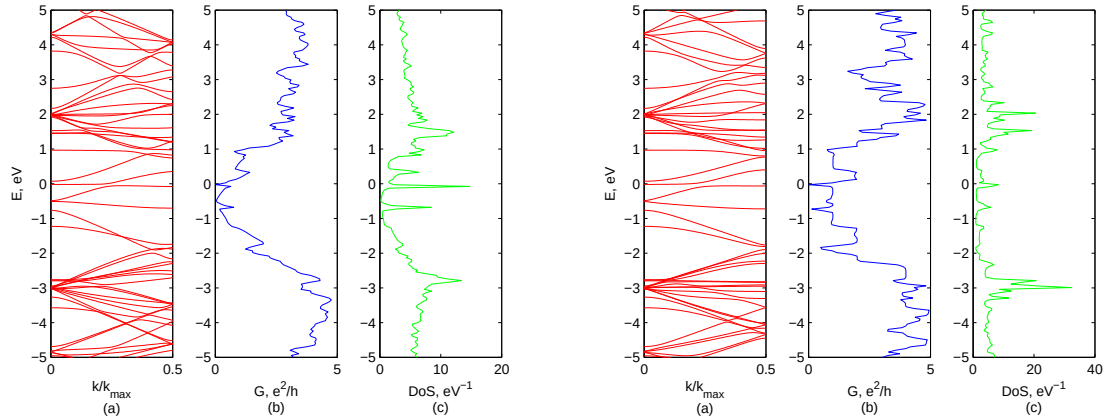

S-ep in Γ-K direction **S-ep in Γ-M direction**

Figure 5. Band structure (a), conduction (b), and density of states (c) of various ep-graphene.

occupying these bands are extremely heavy and do not contribute much to conductance. This analysis is very important for further consideration, especially regarding flat bands appearing in different

functionalization schemes.

Almost all structures still preserve graphene like V-shaped conductance behavior in the vicinity of the former Dirac-point. They are disturbed by the presence of heteroatom levels which despite their small dispersion make some contribution to conductance. The higher the dispersion of these bands, i.e. the higher the degree of functionalization, the higher is the contribution to conductance. That explains the similarity in the band gaps and conductance trends.

That being said, one concludes that the key to band-gap opening and high conductance in such functionalization is the degree of hybridization, i.e. mixing between graphene MOs and MOs of the functionalizing groups. Attempting to accommodate extra electrons donated by the heteroatom, graphene MOs and MOs of the functionalizing groups will hybridize strongly creating more low energy collective MOs. The next step towards enhancement of charge transfer is to bind the heteroatom with another electron donor (acceptor).

4. "ino" Functionalization

Atoms with odd number of valence electrons (B,N,P,etc.) after bonding to graphene sheet still have one dangling bond that can be terminated with hydrogen. This gives rise to a family of "ino"-functionalized graphene. Again, as in the previous paragraph under "ino" we consider a group of radicals, :N̈H - amino, :P̈H - phosphino, :BH - , :CH_2 - carben, :SiH_2 - silene that use one electron pair to bind to the graphene sheet, and hereinafter we refer to their corresponding compounds as N-inographene, P-inographene, B-inographene, etc.

The structure of inographenes was optimized starting from the structure of epgraphene with one H-atom initially placed right above the heteroatom. As a result of optimization the position of the hydrogen atom differed for different electronic structure of the heteroatom. If a heteroatom has a lone pair, like N or P than the angle ∠(H-X-cent), where "cent" stands for the center of the C-C bond to which the heteroatom is attached, decreases from the initial straight-upright configuration, 180° (See Fig. 6), to almost 90°, depending on which AO forms the lone pair (e.g. $1p$ for for nitrogen and $2p$ for phosphorus).

Angle ∠(H-X-cent) declines from 180°, which correspond to sp^3 hybridization of the hetero atom, to almost 90° for P-inographene, since the lone pair acts an additional ligand essentially changing the hybridization from sp^3 to $sp^{2+\eta}$. The rehybridization parameter (η) increases from N to P as the principal quantum number of valence electrons increases. Tetrahedral angles for C- and Si- derivatives, are very similar and slightly higher than the ideal tetrahedral angle (109°), since the bonding environment "on the top" and "on the bottom" is not symmetric, and graphene carbon atoms also have residual binding between each other due to not complete rehybridization from sp^2 to sp^3. Bond lengths in Figure 6 reveal a trend with depression, which is associated with the nitrogen atom since it is the most electronegative element in the B-C-N row. As the size of the heteroatom drastically increases, i.e. by moving from the second period to the third (Si-P), bond lengths undergo a jump, but continue to follow a declining trend.

4.1. Band structure of inographene

Band structures of inographene resemble that of the ep- structures (smallest band gap occurs in the Γ point due to BZ folding). Band structures are shown in Fig. 7, and numerical values of band gaps

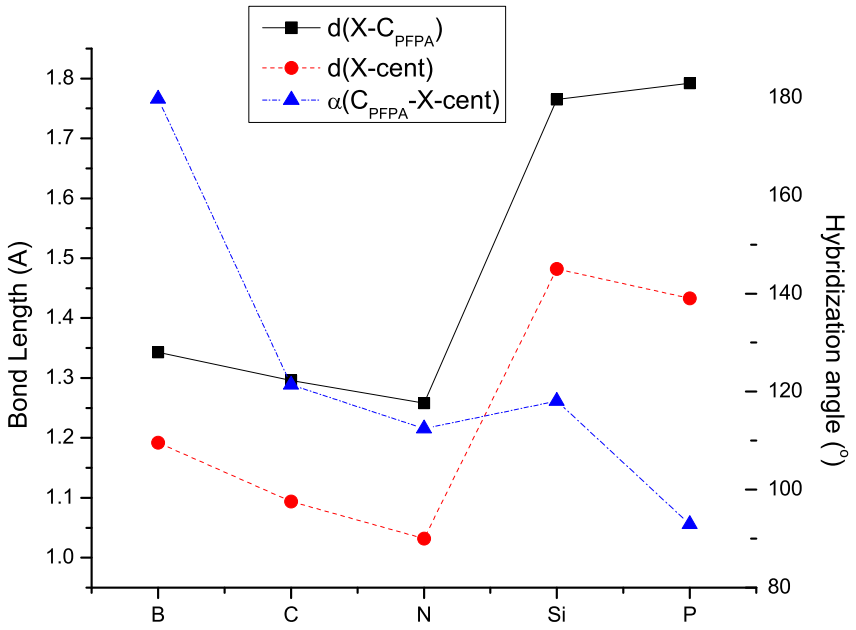

Figure 6. Bond lengths and hybridization angles in aminographene.

are summarize in Table 2 at the end of the chapter.

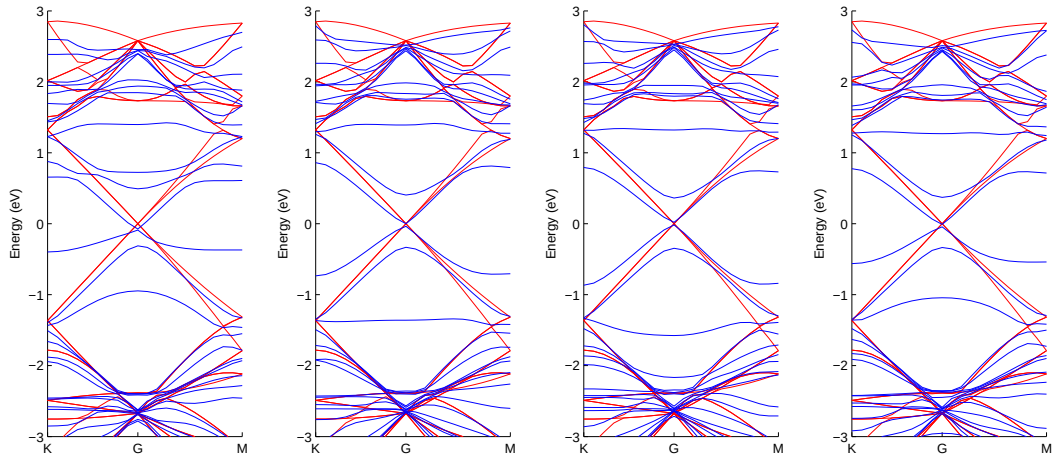

(a) B-inographene **(b) C-inographene** **(c) N-inographene** **(d) P-inographene**

Figure 7. Band structures of pristine (red) and ino-functionalized (blue) graphene. Band structures are aligned with respect to the position of the Fermi level.

Band gaps extracted from Fig. 7 are fairly narrow. Comparing these band gaps with thermal energy at room temperature (300°K≈25meV), we conclude that ino functionalization is hardly of any practical

use[‡]. The reason for such low impact on the π-conjugated structure of graphene is because a heteroatom bonded to a single hydrogen atom cannot accommodate a lot of extra electron density from graphene. This is because hydrogen with only one valence electron and only one hole is neither an efficient donor, nor an efficient acceptor, and it makes the "amino" group a weak functionalizer as well.

In order to enhance acceptor properties we need to attach a substituent to the heteroatom that can spread enough charge to reduce excessive negative charge of the heteroatom. One of such efficient substituents is a phenyl ring because it also possesses π-conjugated structure as well. This phenyl functionalization gives rise to the so called PFPA-FG graphene.

5. PFPA Functionalization

PFPA (perfluorophenylazide) is a benzene molecule with two substituents in the para configuration: azide and possibly another functionalizing group, like methyl, or a C-Si-C chain. (Fig. 8)

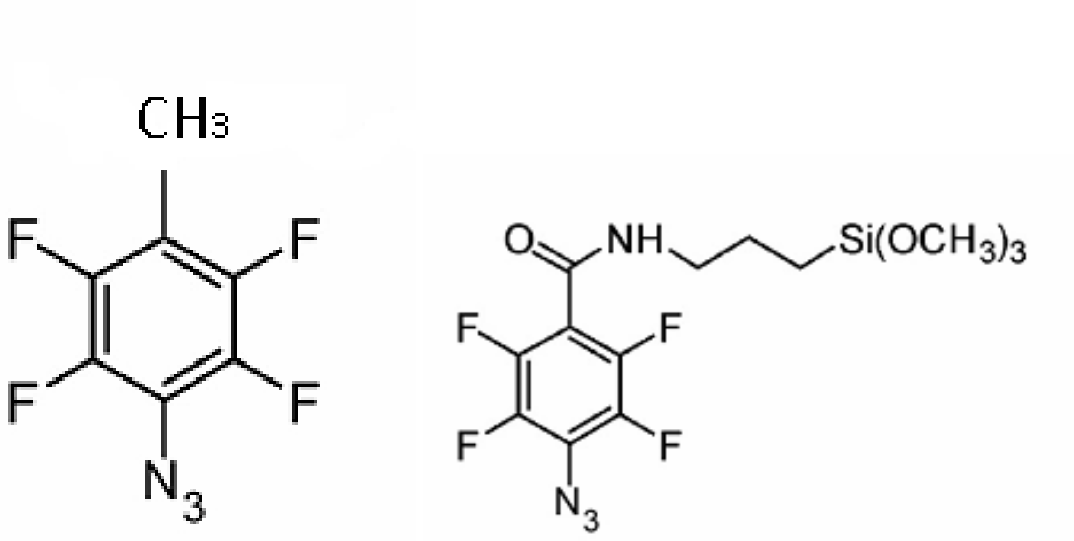

Figure 8. Perfluorophenylazide molecule with methyl and "silane" moieties.

PFPA has drawn widespread interest for functionalizing graphene because of its relatively high reactivity along with its high affinity to graphene's carbon atoms (by the first para substituent). It also has the ability to immobilize graphene to silicon wafers (via second para substitution) and modify its band structure [7, 26, 27].

In order to calculate any structural or electronic properties one first needs to obtain an optimized geometry for both bare PFPA and PFPA functionalized graphene (PFPA-FG). The results of this analysis are reported in one of our previouls papers [28], therfore here we will just briefly summarize the results for the purpose of comparison with other strucutre under consideration.

The strucutre of PFPA graphene is determined by the fact that in this configuration nitrogen has four unshared electrons distributed over two lone pairs. Two of these four electrons form two bonds with carbon atoms of graphene, and the remaining two stay attached to the nitrogen atom as a lone pair. This electron configuration explains optimized geometric structure of PFPA-FG, namely the bending of the

[‡]Except maybe of infrared bolometers, that are operated under cryogenic temperatures.

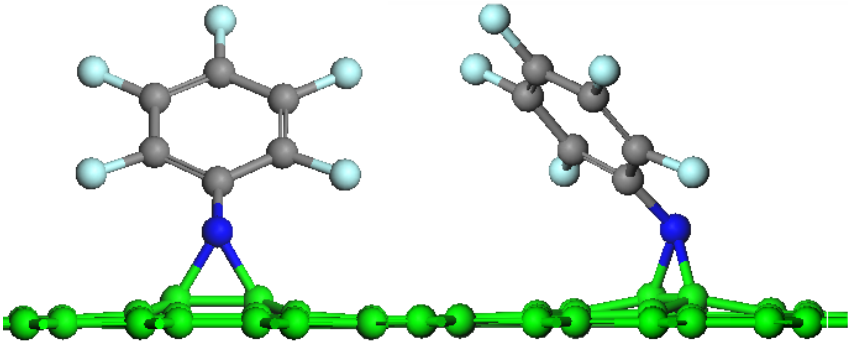

Figure 9. Structure of N-PFPA functionalized graphene. Green - graphene sheet carbon atoms, grey - PFPA carbon atoms, blue - nitrogen, cyan - fluorine.

PFPA molecule with respect to the graphene plane: the nitrogen would prefer trigonal coordination with one of the apexes to the the lone pair (Fig. 9). The same can be observed for the phosphenidene radical, however due an increased atomic volume and the volume of the lone pair, deviation from the upright geometry will be even more significant. The atomic structure of C-PFPA (as well as Si-PFPA), in contrast suggests that there should be two phenyl rings attached to the the carbon "heteroatom" (Fig. 10).

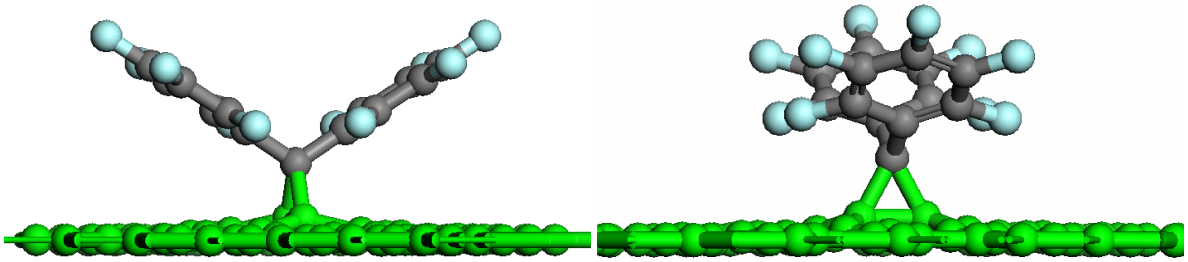

Figure 10. Structure of C-PFPA functionalized graphene. Green - graphene sheet carbon, grey - PFPA carbon, cyan - fluorine.

Geometrical parameters that characterize PFPA-FG structures are the angle ∠(C-X-cent) and d(X-cent). C denotes the carbon atom of the phenyl ring bound to a heteroatom, "cent" - center between two carbons of graphene sheet to which the heteroatom (X) binds. Bonding angles between graphene and heretoatoms decrease almost linearly in the B-N-C-P-As row (Fig. 11 right scale). Bond lengths $d(C-X)$ in Fig. 11, similar to Fig. 6, reveal a trend with a valley (Fig. 11 left scale), which is associated with the nitrogen atom since nitrogen is the most electronegative atom in the B-C-N row. The explanation for this trend is very similar to the ino-graphene case and is not repeated here. However, noticing that C_{PFPA}-X bond length in PFPA-FG are on average 29% longer than in amino-FG, and X-cent are about 2% longer than in corresponding amino structures, i.e. on average bonding to PFPA is weaker than in the ino case. Despite that charge transfer in PFPA-FG structures is slightly ($\sim 5\%$) higher than in ino-FG. It is enough to open a six times wider gap (in case of N - the most efficient covalent functionalizer) in PFPA-FG structures compared to amino-FG. To pursue a detailed explanation of this phenomenon we compare electronic structures of functionalizers of both of these groups.

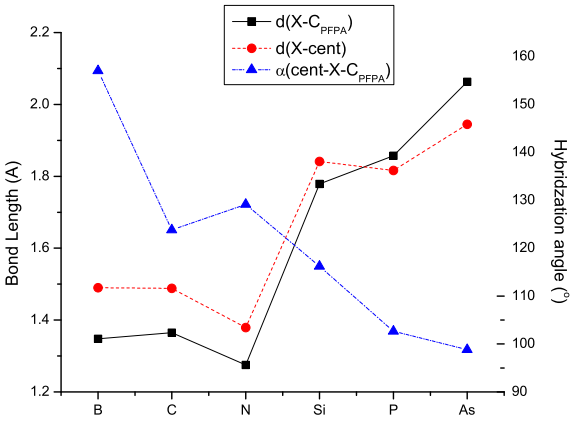

Figure 11. Bond lengths and hybridization angles in PFPA-FG.

5.1. Band structure of PFPA-FG

Acceptor properties increase in the row R-B:, R-P̈:, R-N̈:, and thus we can expect that band gap will follow the same trend, since the width of the gap is proportional to the charge transfer, which increases as electronegativity decreases. Both trends are proportional to the difference between the diagonal elements of the Hamiltonian matrix. A detailed description of that phenomenon resembles that for epoxy- and aminographene and thus is not repeated here.

From Table 2 it can be seen that the widest gap that can be induced in graphene by functionalization with a single PFPA molecule per 6x6 graphene supercell is 0.24eV. Functionalization with two molecules slightly increases the gap to 0.28 eV. This is more than 100 times higher than the thermal energy at room temperature and thus can find industrial application in microelectronics, providing a feasible ON/OFF ratio for transistors.

Band structure of PFPA-FG resembles that of aminographene. Previously intersecting π and π^* bands that formed the Dirac cones are now pulled apart by the underlying σ bands, arising from the interaction of the heteroatom with the system of graphene' sp_z orbitals. This $\sigma - \pi$ interaction causes rehybridization of the carbon atoms from the sp^2 to $sp^{2+\eta}$ state. The degree of additional hybridization (η) is directly related to the band gap, as it was discussed above for epoxygraphene. Unlike e.g. haptic functionalization [30], $sp^2 \longrightarrow sp^3$ rehybridization causes deplanation of graphene structure. In this case degeneracy, that was previously imposed by symmetry on phonon modes, is now removed, and thus the electron phonon scattering is significantly stronger in deplanated structures than is bulk- and/or rigid structures.

Comparing the corresponding band gaps of PFPA- and amino-graphene, one finds that in all cases the gap in PFPA-graphene is larger than in aminographene. The reason for this is probably the ability of a phenyl ring to accommodate a higher electron density, that leads to an increase of the charge transfer through the heteroatom and thus enhances charge transfer from graphene sheets to the functionalizing molecules.

Charge transfer is calculated in the same way as in sec. 4.1. Table 1 demonstrates that the highest charge transfer occurs in N-compounds. Considering the trends in the band gap, the sign of the ΔQ indicates donor or acceptor properties. Charge transfer in turn, depends on the relative (with respect to

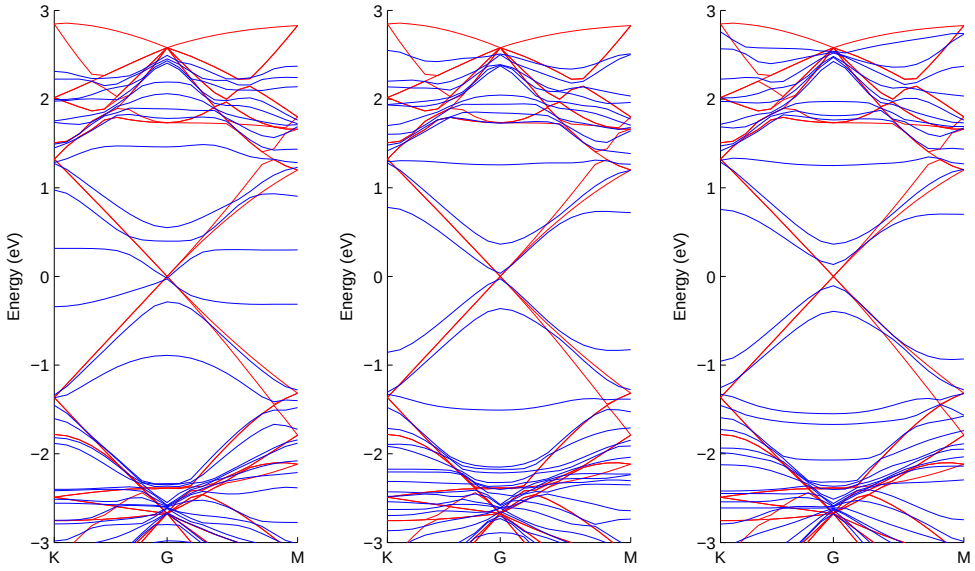

(a) B-PFPAgraphene **(b) C-PFPAgraphene** **(c) N-PFPAgraphene**

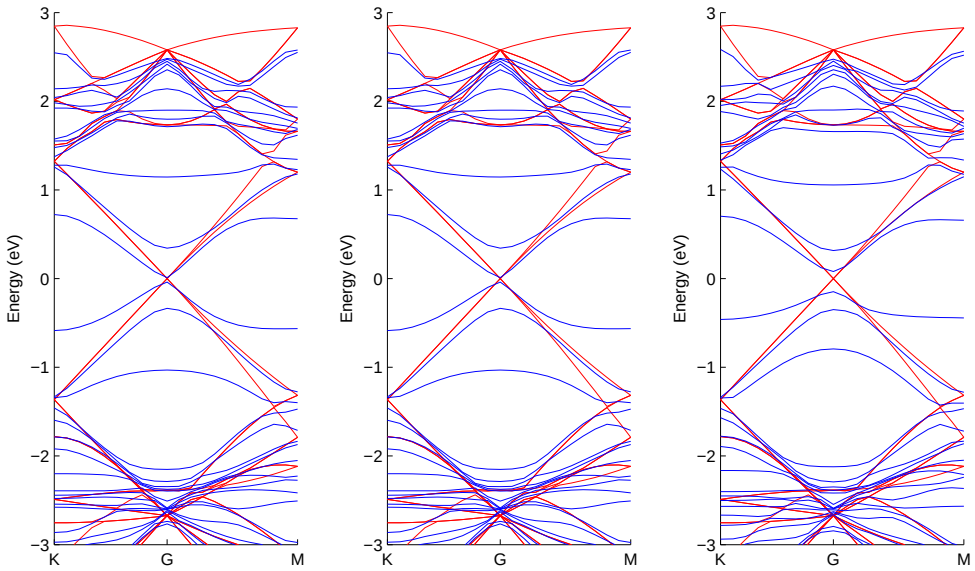

(d) Si-PFPAgraphene **(e) P-PFPAgraphene** **(f) As-PFPAgraphene**

Figure 12. Band structures of pristine (red) and PFPA-functionalized (blue) graphene. Band structures were aligned with respect of the position of the Fermi level of pristine graphene.

carbon) electronegativity of the heteroatom. Strong donors (small relative electronegativity) result in small band gaps (B, P), whereas strong acceptors (high relative electronegativity) result in wider band gaps. Weak donors and acceptors, such as arsenic and carbon result in intermediate values of the band

Table 1. Charge, charge transfer (ΔQ), and relative electronegativity (χ_X/χ_C) in PFPA-FG.

Compound	X	C(up)	C(down)	ΔQ	χ_X/χ_C
B-PFPA	+0.608	-0.151	-0.251/ -0.256	+0.406	0.80
C-PFPA	-0.058	-0.078	-0.075/ -0.075	-0.054	1.00
N-PFPA	-0.277	+0.103	-0.043/ -0.045	-0.314	1.19
P-PFPA	+0.377	-0.431	-0.259/ -0.253	+0.398	0.86
As-PFPA	+0.018	-0.315	-0.186/ -0.174	+0.087	0.85

C(up) stands for the carbon atom from the phenyl ring, linked with the heteroatom,
C(down) stands for two carbon atoms from the graphene sheet, linked with the heteroatom.

gap. Therefore the N-PFPA compound probably possesses the widest band gap among all the possible PFPA-FG compounds. Based on this fact we will focus our transport computations on the transport properties of N-PFPA-FG.

5.2. Wannier functions and transport in PFPA-FG

Since PFPA-functionalization leads to opening of a significant gap in the electron dispersion spectrum of functionalized graphene, the curvature of the top valence and bottom conduction bands at the Γ point now leads to a finite electron mass. Therefore we cannot expect electron mobility to be as high as in pristine graphene.

To understand the nature of mobility degradation caused by functionalization we employed the non-equilibrium Green's functions (NEGF) method using localized Wannier functions as the basis set. For transport calculations, we consider only an infinite sheet with one functionalizing molecule per 6x6 graphene supercell (Fig. 9). In this geometry no boundary states are created and thus the whole scattering is attributed to Coulomb scattering off electron density disturbances and electron-phonon scattering. Narrow (with respect to the size of the PFPA molecule) GNRs functionalized with PFPA are beyond the scope of this paper, since GNRs conventionally produced are usually of the size $\approx 10\mu m$ wide[§]. This corresponds to $\approx 10^4$ honeycombs. At this number of honeycombs BZ folding leads to an almost infinite increase of bands in a very small reciprocal cell, and thus periodic boundary conditions can be imposed in both directions. Also this would allow one to eliminate the effects of boundary scattering and focus on effects of functionalization on electrical conductivity.

Wannier functions of PFPA-FG. A trial set of Wannier functions in PFPA-FG structures was initialized in similar way as described in section 3.2. The graphene subset was initialized as a set of σ-type orbital located between carbon atoms and nonbonding p_z orbitals. The PFPA subset was explicitly defined as a full atomic orbital set (1s+3p orbitals) for the nitrogen atom. The phenyl ring subset is initialized in the same way as graphene: six σ-type orbitals located between carbon atoms, five σ-type orbitals describing C-H bonds, one σ-type orbitals representing C-N bond, and six dangling p_z orbitals, centered on carbon atoms.

The electronic structure of carbon atoms belonging to the graphene subset is, as expected, distorted

[§]Narrower GNRs can be produced by unzipping CNTs [25, 29]

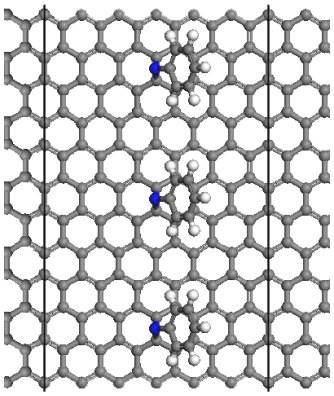

Figure 13. Interface layer of PFPA-FG sandwiched between pristine graphene sheets.

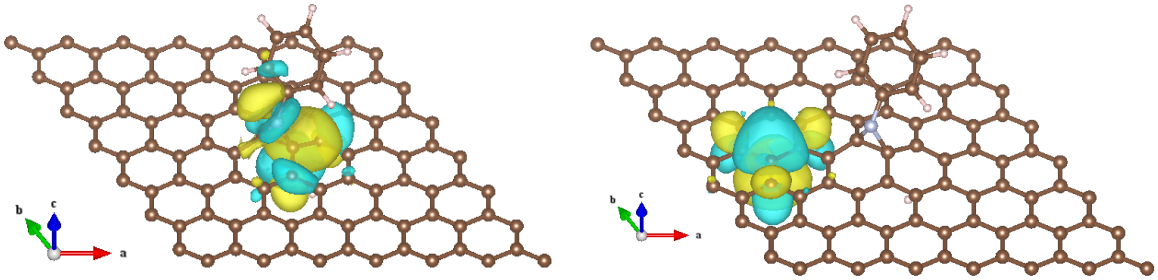

(a) **(b)**

Figure 14. Wannier functions of carbon atoms in N-PFPA-FG. In the direct vicinity of the functionalizing molecule (a) and far away from it (b).

by functionalization (Fig. 14(a)) relative to the atoms located further away from the functionalizing molecule (Fig. 14(b)). This distortion is responsible for the alteration of the band structure and transport properties in functionalized graphene.

Heteroatom (N) interacts with the π-conjugated electron system of graphene with its s and p_z, p_x and p_y orbitals contributing more towards the lone pair and even though it implicitly affects graphene π-structure, its contribution is not significant compared to s and p_z (Fig. 15).

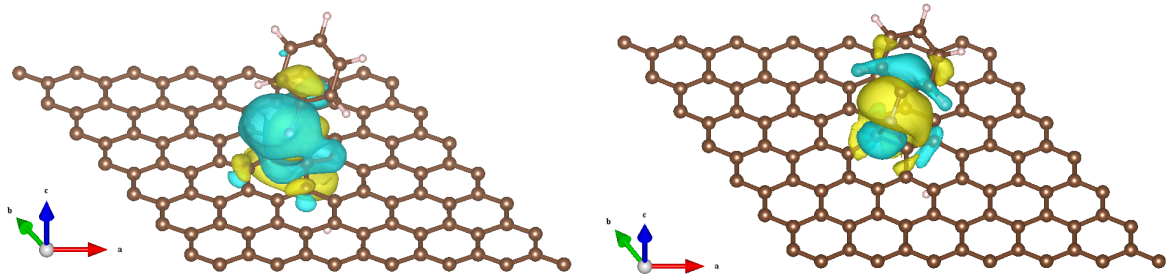

(a) s **(b)** p_z

Figure 15. Wannier functions of the heteroatom in N-PFPA-FG.

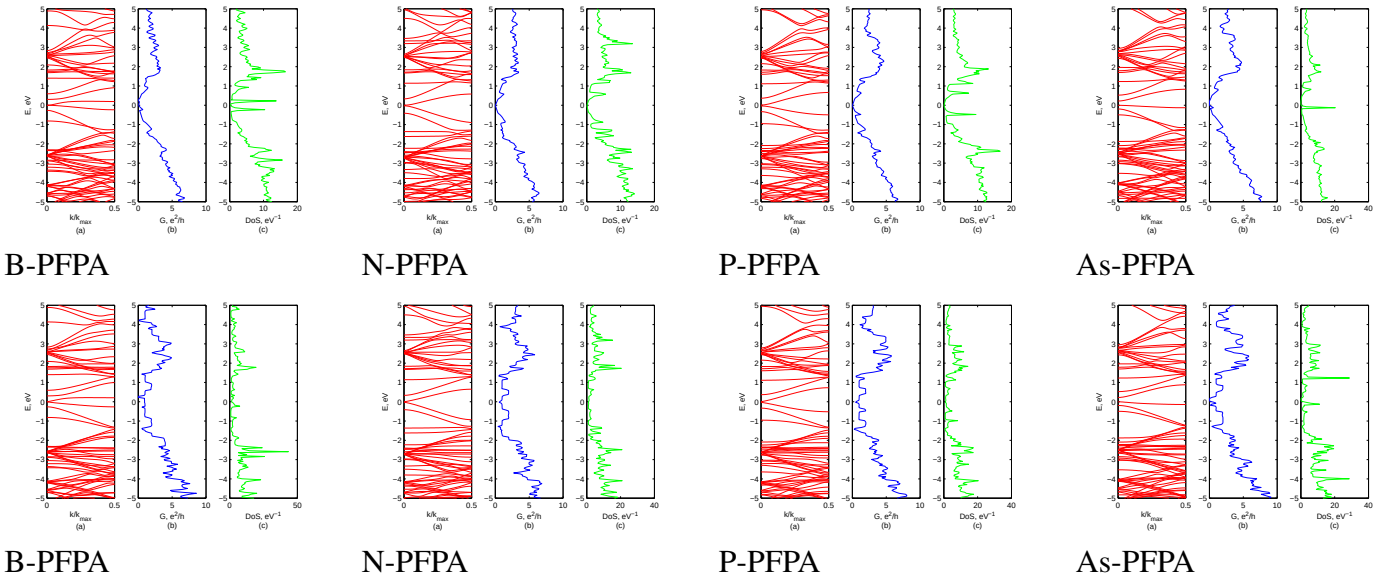

Figure 16. Band structure (a), conductance (b), and density of states (c) of B-, N-, P-, As- PFPA-FG in the Γ-K (top row) and Γ-M (bottom row) directions.

Electric conductivity of PFPA-FG. The set of Wannier functions obtained in the previous section effectively describes the conductivity in energy range ±5eV Conductivity vs bias curves in Fig. 16, exhibit very similar behavior to the transport curves in pristine graphene.

The most pronounced peculiarity of the 1D band structure-conductivity-density of states (BCD) curves in Fig. 16 is the typical conductivity behavior in the vicinity of the former Dirac point demonstrating the same feature (Fig. 20(a)) as that observed in ep-graphene. As before, functionalization creates extra bands in the band structure of functionalized graphene bands. This bands come from molecular levels of the adducts. Depending on the degree of hybridization of those levels with the electronic structure of graphene, they may have different dispersion. In particular, B-, As-, and Si-PFPA-FG creates a flat band in the vicinity of the Fermi level, that does not contribute to the conductivity of these compounds. The N-, P-, and C-PFPA-FG, in turn do not possess those flat bands in their band structure and mainly preserve Dirac cones in their band structure. This has direct influence on conductivity of PFPA-FG compounds. In Fig. 17 we summarize our findings about electric conductivity of PFPA-FG. We plot conductivity as a function of the atomic number of the binding heteroatom. This arrangement may seem not the best one, since all heteroatoms, considered for PFPA functionalization fall intro three clusters of neighboring groups. These can be arranged in different ways: by rows (B-C-N — Si-P — As), or by periods (B — C-Si —N-P-As) of the Periodic Table. However, disregarding which of the possible arrangements is chosen, it can clearly be seen that conductivity follows an ascending trend with saturation.

The highest average conductivity is predicted for As-PFPA-FG, however, the bandgaps (Table 2) are in inverse relation with conductivity. Therefore practical application of PFPA-FG is a trade off between high ON/OFF ratio, supplied by a broad (relative to kT) band gap and electron mobility. Si and C derivatives clearly do no follow the trend observed for B, N, P, As. Functionalization with two PFPA groups, as it occurs in C- and Si-PFPA-FG, actually impedes electron transport even more than a single PFPA functionalization.

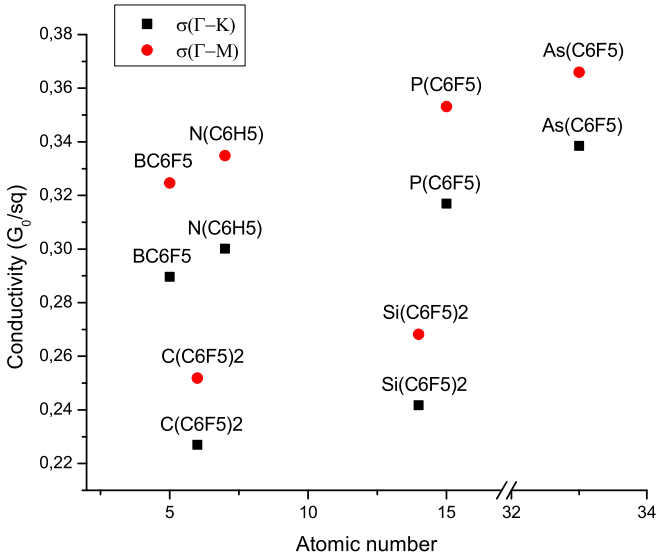

Figure 17. Conductivity of PFPA-FG as a function of the heteroatom.

A general trend observed in figures 16 and 18 is that conductivity in the Γ-M direction is more ballistic (i.e. it deviates less from the eigenmodes count) than in the Γ-K direction. This repeats the picture readily observable in pristine graphene , that it is not significantly disturbed despite functionalization. The BCD pictures for PFPA-FG show that PFPA functionalization as well as epoxy- and amino- functionalization of graphene do not cause any doping, i.e. shift of the minimal conductance point to positive or negative values of electric bias.

5.3. Comparison with experimental results

Typical conductivity behavior in the vicinity of the former Dirac point demonstrate the same feature (Fig. 20(a)) observed in the experimental conductance measurements (Fig. 20(b)).

Only conductance is quantized in multiples of G_0, however, a measurable property of the material is not conductance but conductivity (σ). This consideration becomes especially important when 2D GNRs with different lattice settings are considered, e.g. conductance of graphene in the $\Gamma - K$ direction will be $\sqrt{3}$ times higher in the orthorhombic lattice setting than in the hexagonal due to the fact that the b-lattice parameter, obtained from the lattice transformation is $\sqrt{3}$ times longer than in the hexagonal setting. In case of GNRs due to Brillouin zone folding, the number of bands in the first Brillouin zone increases, also increasing the ballistic conductance. However, since the number of bands is proportional to the number of atoms, which in turn, is proportional to the width of the GNR, conductivity remains same.

Experimental conductivity was measured on a nanoribbon of N-PFPA functionalized graphene. Preparation of the sample has been described elsewhere [9].

Graphene nanoribbons were immobilized by PFPA molecules on a silicon oxide coated silicon wafer. Electrical contacts were fabricated on top of the graphene ribbon by electron beam lithography, followed by thermal evaporation of 40 nm of Cr followed by 60 nm of Au and finally the lift-off process with acetone. Figure 19 shows the fabricated structure. Electrical conductance measured between first and second electrodes was chosen for comparison with the theoretical results.

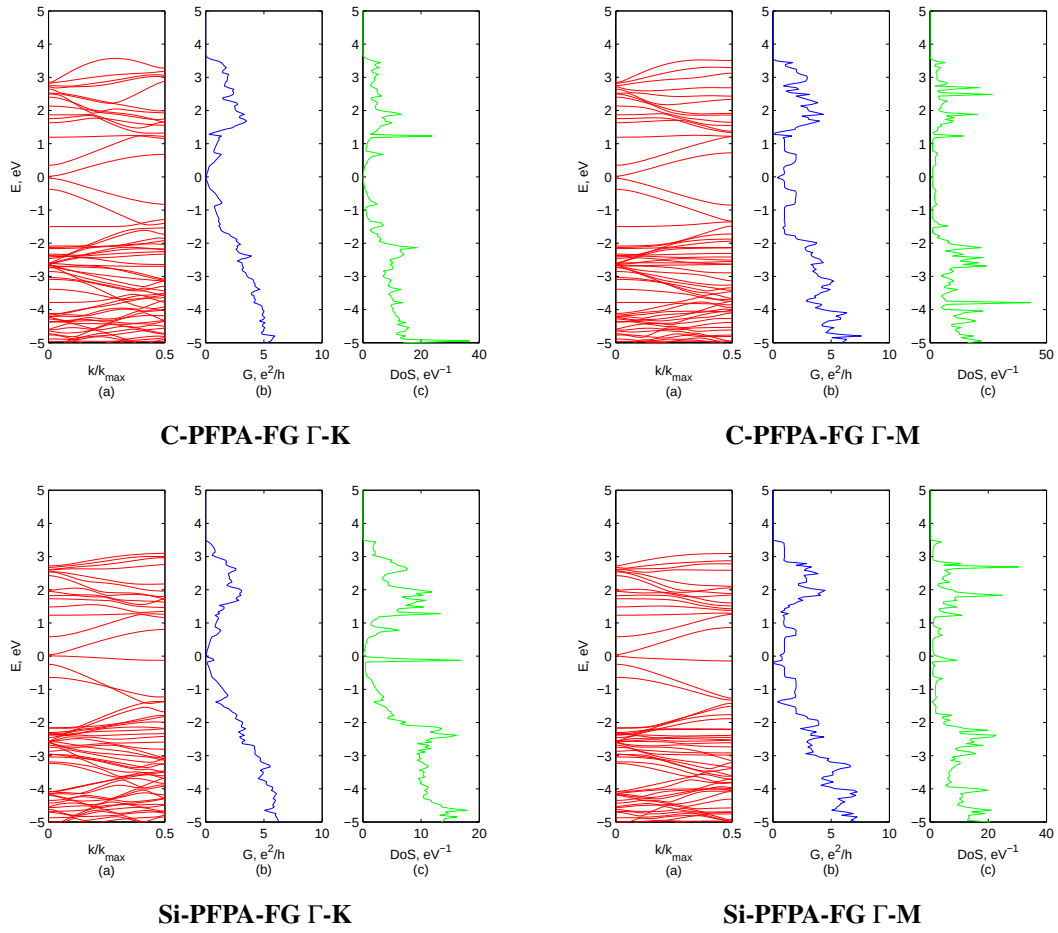

Figure 18. Band structure (a), conduction (b), and density of states (c) of C-, Si- PFPA-FG in the Γ-K (left) and Γ-M (right) directions.

Theoretical conductance (G) was converted to resistivity as: $\rho = S \times \frac{12900\Omega}{G}$, where 12900Ω is the quantum conductance and S is the shape factor. Since the calculations were conducted on a 6×6 hexagonal supercell, and the resistivity refers to the unit area, $S = 6 \times 6 \times \sqrt{3}$. The factor $\sqrt{3}$ comes from conversion of the hexagonal cell metrics into the rectangular structure, suitable for the geometry under consideration. The total resistance between the two electrodes on a graphene film can be modeled as Eq.(1),

$$R = \frac{L}{W}\rho_s + R_c, \tag{1}$$

where ρ_s is the sheet resistance of functionalized graphene, L and W are the channel length and width, respectively, and R_c is the contact resistance between the metal and the graphene ribbon.

By fitting the theoretical sheet resistivity (ρ) to the experimental values (ρ_s) as shown in Fig.19 we obtain a good fit between the shape of the theoretical conductance curve and the experimental one. The unknown R_c was found to be 7422Ω.

The trend demonstrates that N-PFPA functionalization, even though it locally disturbs π-system of pristine graphene still preserves linear conductivity behavior in the vicinity of the charge neutrality point. This suggests that the disturbance of the conjugated electron system by PFPA functionalization

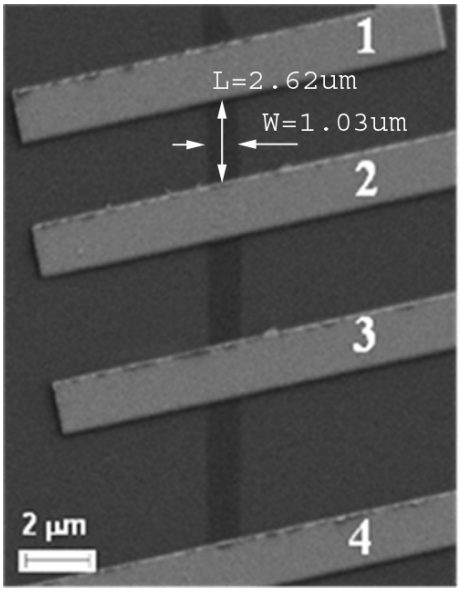

Figure 19. The shape of the functionalized GNR.

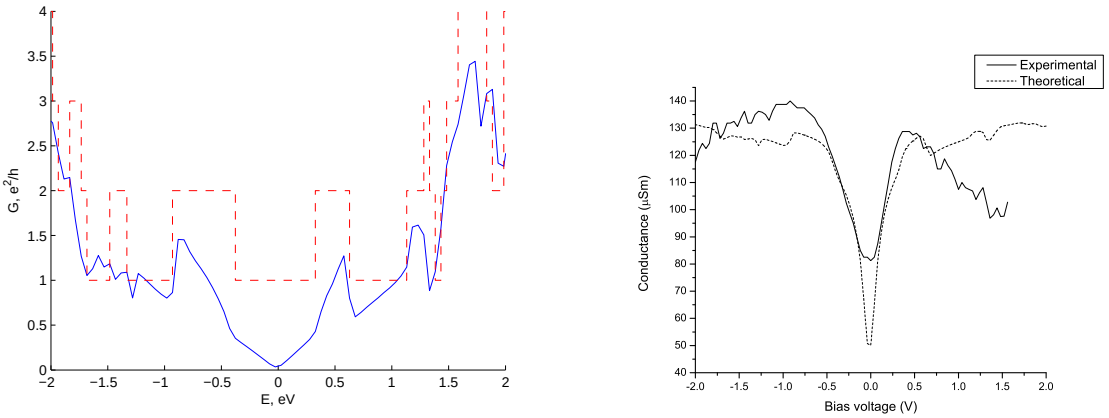

(a) **(b)**

Figure 20. Comparison between theoretical (a) and experimental (b) conductance vs bias voltage curves.

is not very dramatic, indeed the average conductivity in the range of ±5V is just half as that for N-PFPA-FG vs pristine graphene.

Minor discrepancies between the curves is likely due to impurities present in functionalized graphene and on the silicon/ silicon oxide surface. During the fitting procedure the experimental curve was shifted by 0.4V to the left that accounts for the p-doping of functionalized graphene caused by impurities. The position of the Dirac point depends on several factors: the difference between the work functions of the gate and the graphene, the type and density of the charges at the interfaces at the top and bottom of the channel, and any doping of the graphene [31]. Also minimal conductance was found to be 30μSm less than the theoretical limit most likely due to the impurities and less than ideal metal/graphene contacts.

Table 2. Summary of electronic properties produced by covalently functionalization of graphene.

Structures	Band gap (eV)	$\langle\sigma_{\Gamma-M}\rangle$ ($\frac{e^2}{h}/\square$)	$\langle\sigma_{\Gamma-K}\rangle$ ($\frac{e^2}{h}/\square$)	ΔQ (e)
graphene				
Hex	0	0.7037	0.7037	0
Orth	0	0.775279	0.775279	0
Epoxy				
C	27	0.237537	0.278921	-0.025
O	39	0.278077	0.300646	-0.247
S	41	0.28996	0.315328	-0.411
Amino				
BH	14.55			0.339
CH_2	36.15			-0.977
NH	2.47			-0.321
SiH_2	36.49			0.677
PH	34.56			0.251
PFPA				
BC_6F_5	0	0.289671	0.324694	0.406
$C(C_6F_5)_2$	54.42	0.226993	0.2519	-0.054
$N(C_6H_5)$	244.89	0.300124	0.334886	-0.314
$Si(C_6F_5)_2$	27.21	0.241798	0.268179	-0.032
$P(C_6F_5)$	54.42	0.31693	0.353172	0.398
$As(C_6F_5)$	217.68	0.338508	0.365968	0.087

6. Conclusion

In Table 2 we summarize our numerical results: band gaps, average conductivities, charge transfer, obtained for epoxy-FG, amino-FG, and PFPA-FG. Among all covalent functionalizers considered here, the highest band gap is achieved in case of functionalization of graphene by PFPA molecules. Minimal conductivity degradation remains about 50%, and the highest band gap opened in N-PFPA-FG is 0.24eV. This is about 100kT at room temperature and is already somewhat feasible for microelectronic applications. Since there are well established ways of producing of PFPA-FG [7, 8, 9] and it also has been demonstrated [26] that silene-PFPA can be used to immobilize graphene on Si-wafers, PFPA is probably the only way currently available to produce functionalized graphene.

Conflict of Interest

All authors declare no conflicts of interest in this paper.

References

1. Elias DC, Nair RR, Mohiuddin TMG, et al. (2009) Control of Graphene's Properties by Reversible Hydrogenation: Evidence for Graphane. *Science* 323: 610–613.
2. Flores MZS, Autreto PAS, Legoas SB, et al. (2009) Graphene to graphane: a theoretical study. *Nanotechnology* 20: 465704.
3. Leenaerts O, Partoens B, Peeters F (2009) Adsorption of small molecules on graphene. *Microelectron J* 40: 860–862.
4. Liu Z-B, Xu Y-F, Zhang X-L, et al. (2009) Porphyrin and fullerene covalently functionalized graphene hybrid materials with large nonlinear optical properties. *J Phys Chem B* 113: 9681–9686.
5. Choi J, Kim K-J, Kim B, et al. (2009) Covalent Functionalization of Epitaxial Graphene by Azidotrimethylsilane. *J Phys Chem C* 113: 9433–9435.
6. Quintana M, Spyrou K, Grzelczak M, et al. (2010) Functionalization of graphene via 1,3-dipolar cycloaddition. *ACS Nano* 4: 3527–3533.
7. Liu L-H, Yan M (2009) Simple method for the covalent immobilization of graphene. *Nano Lett* 9: 3375–3378.
8. Liu L-H, Zorn G, Castner DG, et al. (2010) A simple and scalable route to wafer-size patterned graphene. *J Mater Chem* 20: 5041.
9. Liu L-H, Nandamuri G, Solanki R, et al. (2011) Electrical Properties of Covalently Immobilized Single-Layer Graphene Devices. *J Nanosci Nanotechnol* 11: 1288–1292.
10. Leenaerts O, Partoens B, Peeters F (2008) Adsorption of H2O, NH3, CO, NO2, and NO on graphene: A first-principles study. *Phys Rev B* 77: 125416.

11. Leenaerts O, Partoens B, Peeters F (2008) Paramagnetic adsorbates on graphene: A charge transfer analysis. *Appl Phys Lett* 92: 243125.
12. Erni R, Rossell M, Nguyen M-T, et al. (2010) Stability and dynamics of small molecules trapped on graphene. *Phys Rev B* 82: 165443.
13. Zólyomi V, Rusznyák A, Koltai J, et al. (2010) Functionalization of graphene with transition metals. *Phys Status Solidi B* 247: 2920–2923.
14. Park H, Zhao J, Lu JP ()2006 Effects of sidewall functionalization on conducting properties of single wall carbon nanotubes. *Nano Lett* 6: 916–919.
15. Calzolari A, Marzari N, Souza I, et al. (2004) Ab initio transport properties of nanostructures from maximally localized Wannier functions. *Phys Rev B* 69: 035108.
16. Dubois S-M, Zanolli Z, Declerck X, et al. (2009) Electronic properties and quantum transport in Graphene-based nanostructures. *Eur Phys J B* 72: 1–24.
17. Schedin F, Geim A, Morozov S, et al. (2007) Detection of individual gas molecules adsorbed on graphene. *Nat Mater* 6: 652–655.
18. Saxena AP, Deepa M, Joshi AG, et al. (2011) Poly(3,4-ethylenedioxythiophene)-ionic liquid functionalized graphene/reduced graphene oxide nanostructures: improved conduction and electrochromism. *ACS Appl Mater Interface* 3: 1115–1126.
19. Delley B (2000) From molecules to solids with the DMol approach. *J Chem Phys* 113: 7756.
20. Becke A (1988) Density-functional exchange-energy approximation with correct asymptotic behavior. *Phys Rev A* 38: 3098.
21. Lee C, Yang W, Parr RG (1988) Development of the Colle-Salvetti correlation-energy formula into a functional of the electron density. *Phys Rev B* 37: 785.
22. Vosko SH, Wilk L, Nusair M (1980) Accurate spin-dependent electron liquid correlation energies for local spin density calculations: a critical analysis. *Can J Phys* 58: 1200–1211.
23. Saito R, Dresselhaus G, Dresselhaus M, et al. (1998) Physical properties of carbon nanotubes, volume 3. London, Imperial College Press London.
24. Wallace P (1947) The Band Theory of Graphite. *Phys Rev* 71: 622–634.
25. Kutana A, Giapis KP (2008) Analytical carbon-oxygen reactive potential. *J Chem Phys* 128: 234706.
26. Loh KP, Bao Q, Ang PK, et al. (2010) The chemistry of graphene. *J Mater Chem* 20: 2277.
27. Suggs K, Reuven D, Wang X (2011) Electronic Properties of Cycloaddition-Functionalized Graphene. *J Phys Chem C* 115: 33133317.
28. Plachinda P, Evans D, Solanki R (2012) Thermal conductivity of graphene nanoribbons: effect of the edges and ribbon width. *J Heat Transfer* 134: 122401.

29. Kosynkin DV, Higginbotham AL, Sinitskii A, et al. (2009) Longitudinal unzipping of carbon nanotubes to form graphene nanoribbons. *Nature* 458: 872–876.

30. Plachinda P, Evans D, Solanki R (2013) Electrical conductivity of PFPA functionalized graphene. *Solid State Electronics* 79: 262–267.

31. Schwierz F (2010) Graphene transistors. *Nat Nanotechnol* 7: 487–496.